Supporting Information for

RNA-based fluorescent biosensors for live cell imaging of second messengers cyclic di-GMP and cyclic AMP-GMP

Colleen A. Kellenberger, Stephen C. Wilson, Jade Sales-Lee, and Ming C. Hammond

Contents:

Materials and Methods

Reagents and oligonucleotides

DNA oligonucleotides were purchased from Elim Biopharmaceuticals (Hayward, CA) and IDT (Coralville, IA). Cyclic di-GMP, cyclic di-AMP, cyclic GMP, and pGpG were purchased from Axxora, LLC (Farmingdale, NY). DFHBI was purchased from Lucerna (New York, NY) and was prepared as a 20 mM stock solution in DMSO. Commercially available reagents were used without further purification. Chemically competent BL21 (DE3) Star cells were purchased from Life Technologies (Carlsbad, CA). *Vibrio cholerae* genomic DNA and D70E WspR DNA were gifts from the Marletta lab.

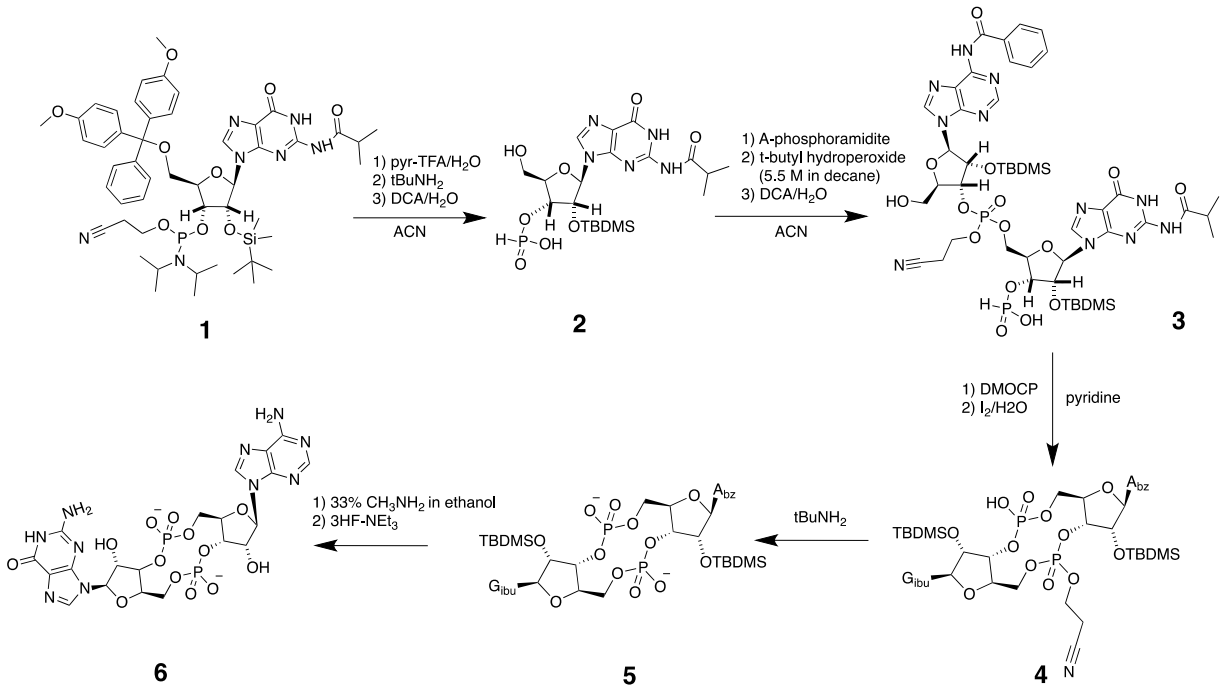

Synthesis of cyclic AMP-GMP (6)

Cyclic AMP-GMP was synthesized using the one-pot procedure from Gaffney *et al.*[1] with the following modification to the work-up of intermediate **5**. After deprotection of **4** with *tert*-butylamine, the crude mixture was concentrated, then washed twice with acetonitrile to remove excess *tert*-butylamine and dried. The residue was subsequently dissolved in methanol and filtered to remove solid impurities. The saved filtrate was concentrated, precipitated again with acetonitrile, and the solid material was filtered and saved. Compound **5** was purified as the di-ammonium salt using reverse-phase HPLC on a Perkin Elmer Series 200 HPLC equipped with a Perkin Elmer Prep 10-ODS C18 column (20 μm, 250 mm x 10 mm, 300 Å). Conditions used were an 85 to 45% gradient of solvent A over 30 min, flow rate 3 mL/min, where solvent A is 100 mM ammonium acetate in water and solvent B is acetonitrile. Purified elution fractions were lyophilized overnight followed by repeated rounds of dissolution and evaporation with methanol in order to remove excess ammonia.

Characterization of **5** (isolated as di-ammonium salt). ^{1}H NMR (600 MHz, d4-MeOD, δ): 8.84 (1H, s), 8.71 (1H, s), 8.35 (1H, s), 8.06 (2H, J = 7 Hz, d), 7.63 (1H, J = 7 Hz, t), 7.54 (2H, J = 7 Hz, t), 6.15 (1H, s), 5.96 (1H, s), 4.85 (2H, m), 4.74 (1H, J = 3 Hz, d), 4.53 (1H, J = 4 Hz, d), 4.52 (1H, d), 4.44 (1H, J = 9, d), 4.40 (1H, J = 11, d), 4.34 (1H, J = 8, d), 4.08 (1H, J = 11 Hz, d), 4.04 (1H, J = 11, d), 2.78 (1H, m), 1.21 (3H, J = 7, d), 1.19 (3H, J = 7, d), 1.04 (9H, s), 0.99 (9H, s), 0.37 (3H, s), 0.31 (3H, s), 0.28 (3H, s) 0.25 (3H, s); ^{13}C {^{1}H decoupled} NMR (600 MHz, d4-MeOD, δ): (all resonances are singlets) 181.77, 168.22, 157.80, 153.05, 150.69, 149.85, 149.48, 143.27, 139.57, 134.89, 133.91, 129.76, 129.47, 125.18, 121.32, 92.16, 91.20, 81.02, 77.355, 77.292, 71.90, 71.87, 63.54, 36.79, 26.53, 19.60, 19.20, 19.09, 18.99, -3.87, -3.93, -4.54, -4.60; ^{31}P {^{1}H decoupled} NMR (600 MHz, d4-MeOD, δ): (all resonances are singlets) -2.20, -2.52; HRMS (*m/z*): $[M-H]^-$ calculated for $C_{43}H_{62}N_{10}O_{15}P_2Si_2$, 1075.3332; found, 1075.3279. $[M+Na-2H]^-$ calculated for $C_{43}H_{62}N_{10}O_{15}P_2Si_2$, 1097.3151; found, 1097.3113.

Characterization of **6** (isolated as 3:2 triethylamine:**6**). ^{1}H NMR (600 MHz, D_2O, 50 °C, δ): 8.70 (1H, s), 8.50 (1H, s), 8.40 (1H, s), 6.41 (1H, br d), 6.25 (1H, br d), 5.28-5.24 (2H, br m), 5.15 (1H, br m), 5.04 (1H, br m), 4.74 (4H, m), 4.39 (2H, J = 2 Hz, t); ^{13}C {^{1}H decoupled} NMR (600 MHz, D_2O, 50 °C, δ): (all resonances are singlets) 157.32, 154.19, 154.04, 151.39, 149.80, 147.81, 140.10, 136.63, 118.85, 115.43, 90.57, 90.05, 80.62, 80.28, 73.71, 70.62, 62.62, 62.51; ^{31}P {^{1}H decoupled} NMR (600 MHz, D_2O, 50 °C, δ): (all resonances are singlets) -1.23, -1.41; HRMS (*m/z*): $[M-H]^-$ calculated for $C_{20}H_{24}N_{10}O_{13}P_2$, 673.0921; found, 673.0926.

In vitro transcription

DNA templates were made through PCR amplification from the appropriate plasmid DNA using primers that added the T7 polymerase promoter sequence (see **Table S1** for primer sequences). The templates were transcribed using T7 RNA polymerase in 40 mM Tris-HCl, pH 8.0, 6 mM $MgCl_2$, 2 mM spermidine, and 10 mM DTT. RNA was purified in a denaturing (7.5 M urea) 6% polyacrylamide gel and was extracted from gel pieces using Crush Soak buffer (10 mM Tris-HCl, pH 7.5, 200 mM NaCl and 1 mM EDTA, pH 8.0). RNAs were precipitated with ethanol, resuspended in TE buffer (10 mM Tris-HCl, pH 8.0, 1 mM EDTA) and their concentrations were determined.

Ligand binding assays

To measure the fluorescence of each RNA construct in response to ligand, a solution of ligand (100 μM) and DFHBI (10 μM) was prepared in buffer containing 40 mM HEPES, pH 7.5, 125 mM KCl, and 3 mM $MgCl_2$. The RNA was renatured in buffer at 70 °C for 3 min and cooled to ambient temperature for 5 min prior to addition to the reaction solution at a final concentration of 100 nM. Duplicate 100 μL binding reactions were incubated at 37 °C in a Corning Costar (Tewksbury, MA) 96-well black plate until equilibrium was reached (see activation curves in Supplementary Figures). The fluorescence emission was measured using a Molecular Devices SpectraMax M3 plate reader (Sunnyvale, CA) with the following instrument parameters: 460 nm excitation, 500 nm emission, 495 nm cutoff. The background fluorescence of the buffer without DFHBI was subtracted from each sample to determine the relative fluorescence units. For experiments to measure K_d, the ligand concentration was varied as the

concentrations of RNA (30 nM unless otherwise noted) and DFHBI (10 μM) were held constant, and the fluorescence of the sample with no ligand was subtracted to determine relative fluorescence units.

Activation and deactivation assays

The rate of activation of fluorescence was measured as described previously[2]. Briefly, a solution of ligand (100 μM) and DFHBI (10 μM) was prepared in buffer containing 40 mM HEPES, pH 7.5, 125 mM KCl, and 3 mM $MgCl_2$ and was warmed to 37 °C. The RNA (100 nM) was renatured in buffer at 70 °C for 3 min then cooled to 37 °C prior to addition to the reaction solution. Immediately after the RNA was added, the fluorescence emission was measured every 2.5 min at 37 °C using the same plate reader settings as for the ligand binding assays. The fluorescence of the sample with no ligand was subtracted to determine relative fluorescence units. The same experiments were carried out with WT Vc2-Spinach (3 nM) or G20A Vc2-Spinach (10 nM) at 25 °C in a buffer containing 10 mM $MgCl_2$ to determine the activation rate at ambient temperature.

Deactivation assays were performed using buffer exchange to remove the cyclic di-nucleotide ligand. RNA (100 nM) was mixed with ligand (10 μM) and DFHBI (10 μM) in a buffer containing 40 mM HEPES, pH 7.5, 125 mM KCl, and 3 mM $MgCl_2$ at 37 °C. Once the reaction had reached maximum fluorescence, half of the reaction was passed through an Illustra NAP-5 column (GE Healthcare) that had been equilibrated with DFHBI (10 μM) in buffer while the other half was passed through the column that had been equilibrated with ligand (10 μM), DFHBI (10 μM), and buffer. Immediately after elution of the RNA, the fluorescence emission was measured every 2.5 min at 37 °C using the same plate reader settings as for the ligand binding assays.

Live cell imaging of *E. coli*

For stable RNA expression *in vivo*, the human $tRNA^{Lys}_3$ scaffold was added to the 5' and 3' ends of WT Vc2-Spinach, as described in Paige *et al.*[2,3]. The WT Vc2-Spinach tRNA construct was amplified using primers that added a BglII restriction site and the T7 polymerase promoter sequence to the 5' end and a T7 terminator and XhoI restriction site to the 3' end. The product was then cloned into the pET31b vector for inducible expression in *E. coli*. Vc2-Spinach tRNA mutants were created by PCR amplification of the appropriate Vc2-Spinach sequence using primers that added EagI and SacII restriction sites to the 5' and 3' ends, respectively. Then the WT Vc2-Spinach fragment was removed from pET31b-tRNA by digestion with EagI and SacII and the appropriate Vc2-Spinach variant was cloned in its place. The WspR gene was amplified using primers that added NdeI and XhoI restriction sites to the 5' and 3' ends, respectively, and the product was cloned into pET24a. The DncV gene was amplified using primers that added an NheI restriction site to the 5' end and a 6xHis tag followed by a XhoI restriction site to the 3' end. This product was then cloned into pET24a for inducible expression in *E. coli*. Quikchange (Stratagene, La Jolla, CA) was used according to the manufacturer's protocol to produce the various mutations.

BL21 (DE3) Star *E. coli* cells were co-transformed with 60 ng each of the appropriate plasmids and cells were plated on LB/Carb/Kan plates (Carb: 50 μg/mL, Kan: 50 μg/mL). Single colonies were used to inoculate overnight LB/Carb/Kan cultures grown at 37 °C. Fresh LB/Carb/Kan cultures were inoculated with the overnight culture, and the cells were induced with 1 mM isopropyl β-D-1-thiogalactopyranoside (IPTG) once they reached an OD_{600} ~ 0.5. Induced cells were incubated for another 2.5 h at 37 °C, then were pelleted, washed once with M9 minimal media, pH 6.5, and resuspended in 200 μL M9 minimal media, pH 6.5 to an OD_{600} ~ 1. The cell suspension was pipetted onto poly D-Lysine coated coverslips and incubated at 37 °C for 45 min to allow the cells to adhere. Unattached cells were removed by washing thoroughly with M9 minimal media, and then 200 μL of 200 μM DFHBI in M9 minimal media, pH 6.5 was added to cover the cells. The cells were incubated with DFHBI on the coverslip for 1.5 h at 37 °C before placing them over microscope slides for visualization. Epifluorescence imaging experiments were performed using a Zeiss 200M AxioVert microscope (Zeiss, Jena, Germany) equipped with a mercury light source X-Cite 120 Series (Exfo Life Science Divisions, Ontario, Canada), a 63x/1.4 Plan-Apochromat oil DIC objective lens and a 1.6x tube lens. For monitoring fluorescence, a GFP filter set with an excitation 470/40 BP, FT 495 beamsplitter, and emission 525/50 BP was used (Filter Set 38 HE).

Fluorescence microscope images were normalized to the brightest sample of the entire set using ImageJ software (NIH, Bethesda, MD). This was done by automatically adjusting the brightness/contrast followed by manually setting the maximum brightness to be the same as the brightest sample.

Image analysis and fluorescence quantitation was carried out using ImageJ software. Cells were manually outlined in the differential interference contrast (DIC) image and saved as individual regions of interest (ROIs). The ROIs were overlaid on the corresponding fluorescence image to measure the mean fluorescence for each cell in the image. The average fluorescence of the black background (e.g. DFHBI solution) was determined for each image and subtracted from the value for each cell to determine the mean fluorescence intensity. At least 50 cells were analyzed to measure the average mean fluorescence intensity. Statistical significance of difference in fluorescence was assessed using a student's t test.

Northern Blot Analysis

Total RNA was isolated using the TRIzol Max Bacterial RNA Isolation Kit (Life Technologies, Carlsbad, CA) from cells grown for 2.5 h after IPTG induction, as described above. Total RNA (~500 ng) was separated on a 9% urea-PAGE gel and the gel was transferred to a Hybond N membrane. After crosslinking, prehybridization was carried out for 4 h at 37 °C in Church's buffer (0.5 M Na_2HPO_4, 0.27 M, NaH_2PO_4, 6% SDS, 2 mM EDTA, and 1% BSA) with 15% formamide. Membranes were incubated with 25 ng ^{32}P-labeled DNA oligo for 6 h before washing with SSC buffer (3 M NaCl, 0.3 M sodium citrate, pH 7) and exposing on a phosphorimager. Quantitative analysis of the blot was performed using ImageQuant (GE Healthcare, Waukesha, WI).

Additional Background on the Spinach Aptamer

The Spinach aptamer was developed by Jaffrey and coworkers[4] through multiple rounds of *in vitro* selection to bind the molecule 3,5-difluoro-4-hydroxybenzylidene imidazolinone (DFHBI), which is an analog of the 4-hydroxybenzilidene imidazolinone (HBI) fluorophore found in GFP. When Spinach binds to DFHBI, it presumably stabilizes the excited state of the fluorophore by preventing non-radiative modes of decay and greatly increases the fluorescence emission. Thus, DFHBI binding to Spinach RNA leads to fluorescence activation.

Furthermore, Jaffrey and coworkers showed that the function of Spinach was dependent on the structure of the second stem loop, but not the sequence. Thus, the second stem loop of Spinach can be replaced with other natural and unnatural small molecule aptamers, such as an ATP aptamer or an S-adenosylmethionine (SAM) riboswitch aptamer, connected through a transducer stem to Spinach.[2] In each of these cases, ligand binding to the appended aptamer causes stabilization of the transducer stem, which renders the Spinach aptamer competent to bind DFHBI. As a result, fluorescence becomes dependent on the presence of the small molecule ligand.

Supplementary Results

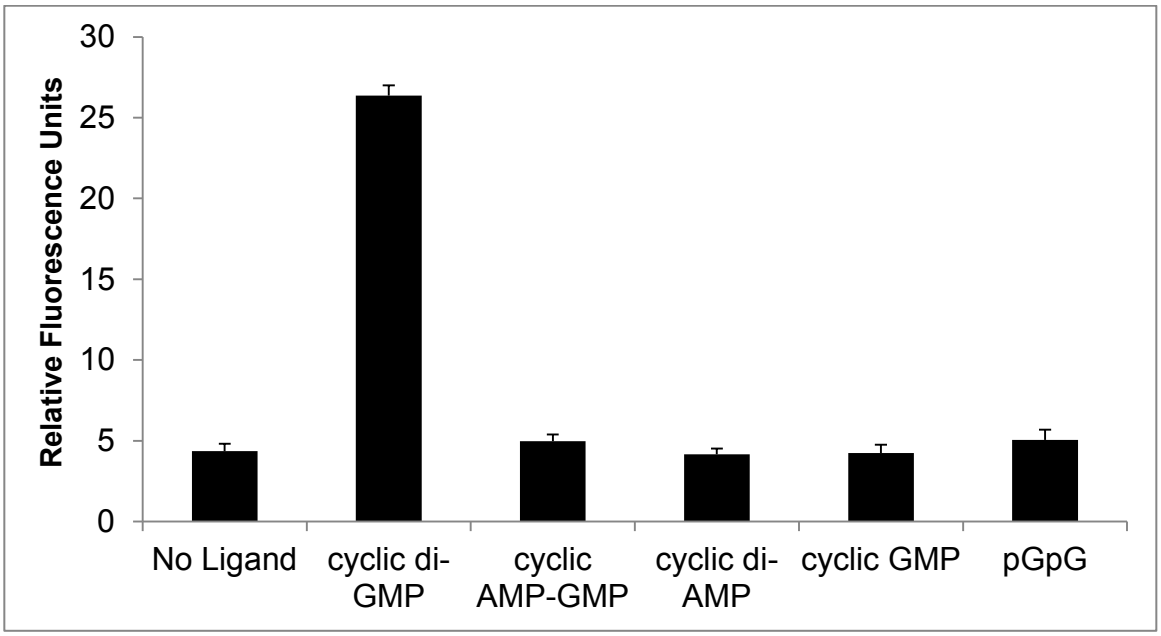

Figure S1. WT Vc2-Spinach is selective for cyclic di-GMP. WT Vc2-Spinach (100 nM) was incubated with ligand (100 μM) and DFHBI (10 μM) at 37 °C in 40 mM HEPES, pH 7.5, 125 mM KCl, and 3 mM $MgCl_2$. Error bars represent the standard deviation of two independent replicates with duplicate samples.

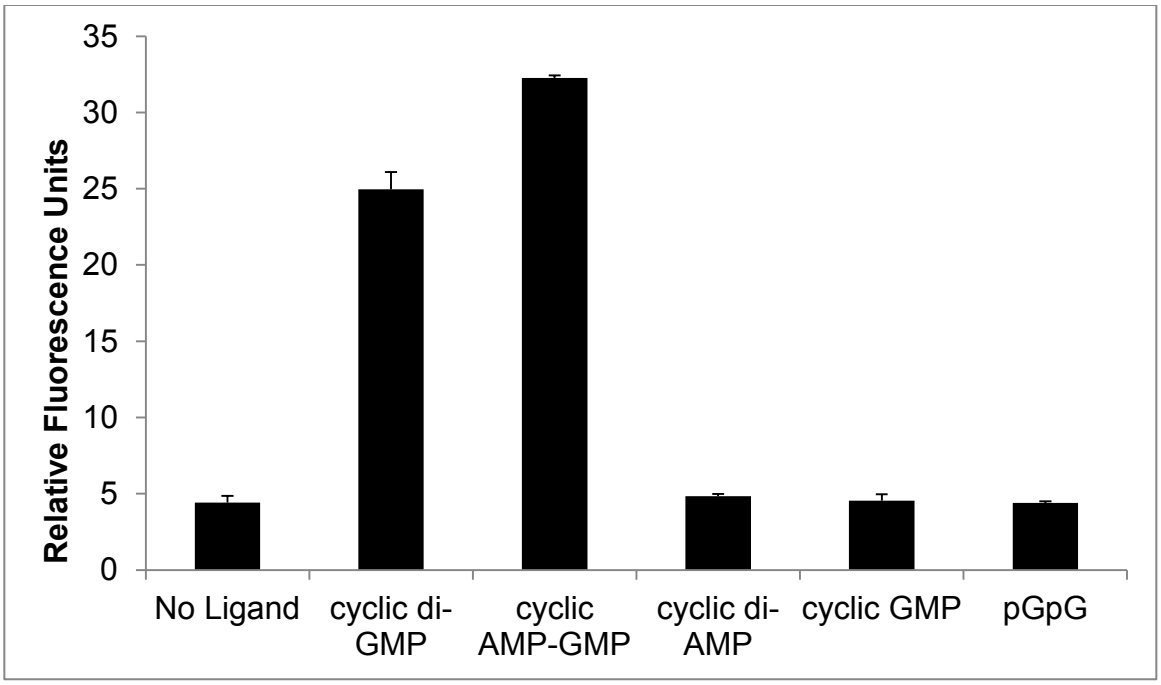

Figure S2. G20A Vc2-Spinach responds to cyclic di-GMP and cyclic AMP-GMP but not to related compounds. G20A Vc2-Spinach RNA (100 nM) was incubated with ligand (100 μM) and DFHBI (10 μM) at 37 °C in 40 mM HEPES, pH 7.5, 125 mM KCl, and 3 mM $MgCl_2$. Error bars represent the standard deviation of two independent experiments with duplicate samples.

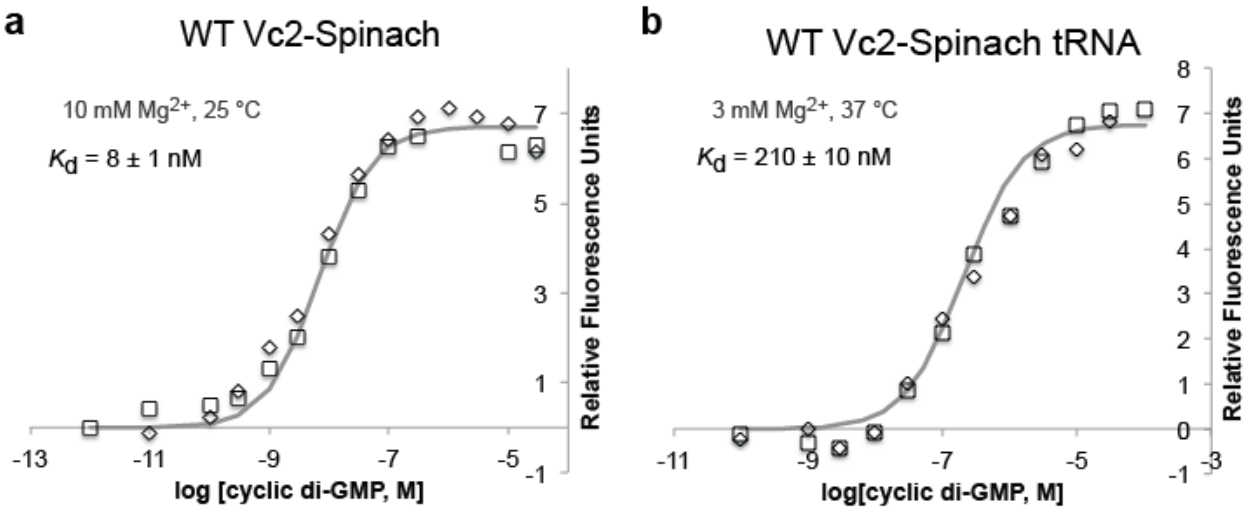

Figure S3. Effect of temperature, Mg^{2+} concentration, and the tRNA scaffold on the affinity of WT Vc2-Spinach. (a) Analysis of WT Vc2-Spinach binding to cyclic di-GMP at 25 °C in 40 mM HEPES, pH 7.5, 125 mM KCl, and 10 mM $MgCl_2$. RNA (3 nM) was incubated with DFHBI (10 μM) and different concentrations of cyclic di-GMP. (b) Analysis of WT Vc2-Spinach tRNA binding to cyclic di-GMP at 37 °C in 40 mM HEPES, pH 7.5, 125 mM KCl, and 3 mM $MgCl_2$. RNA (30 nM) was incubated with DFHBI (10 μM) and different concentrations of cyclic di-GMP. For (a) and (b), data from two independent replicates with duplicate samples and the best-fit curve are shown. Background fluorescence (without cyclic di-nucleotide) was subtracted from all data points.

By lowering the temperature and increasing the concentration of Mg^{2+}, the apparent K_d value of the WT Vc2-Spinach aptamer for cyclic di-GMP decreases. The apparent K_d of WT Vc2-Spinach for cyclic di-GMP is 8 ± 1 nM at 25 °C in buffer containing 10 mM $MgCl_2$, compared to 230 ± 50 nM at 37 °C in buffer containing 3 mM $MgCl_2$. This is likely due to increased folding stability of the RNAs at a lower temperature and with higher Mg^{2+}, as discussed in the main text. The addition of the tRNA scaffold to the WT Vc2-Spinach sequence appears to have no significant effect on the measured K_d.

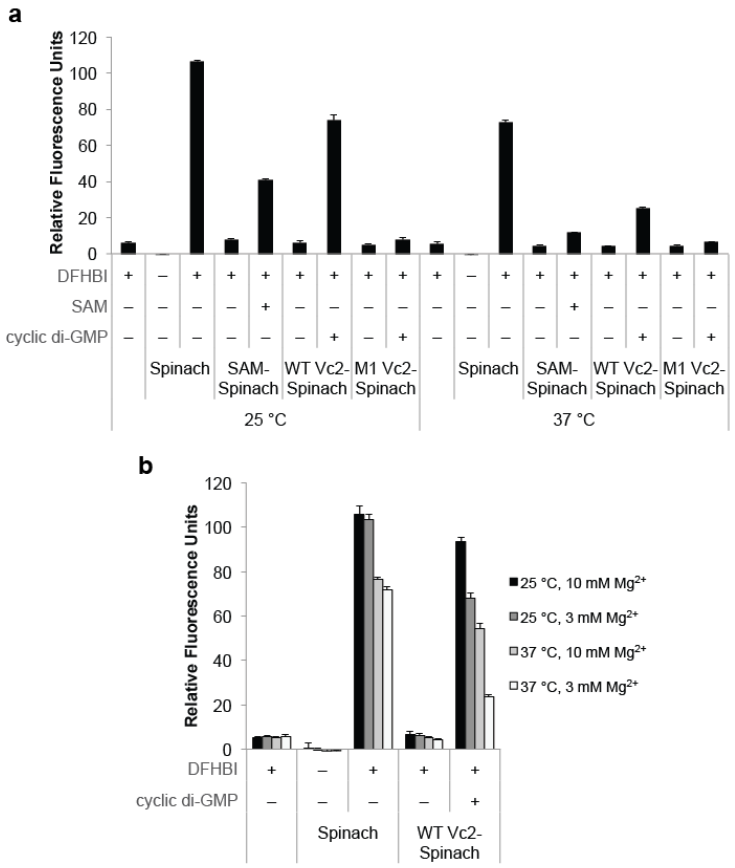

Figure S4. Effect of temperature and Mg^{2+} concentration on fluorescence activation of Spinach constructs. (a) Comparison of fluorescence activation between the original Spinach aptamer and several Spinach-derived biosensor constructs at 25 and 37 °C. The *S*-adenosylmethionine (SAM)-Spinach biosensor was published by Paige *et. al.* See main text for description of Vc2-Spinach constructs. RNA (100 nM) was incubated with ligand (100 μM cyclic di-GMP or 1 mM SAM) and DFHBI (10 μM) in binding buffer. Error bars represent the standard deviation of two independent experiments with duplicate samples. (b) Comparison of the effects of temperature and Mg^{2+} concentration between the original Spinach aptamer and WT Vc2-Spinach. Same reaction conditions as described in (a). Error bars represent the standard deviation of two independent experiments with duplicate samples.

Overall, the biosensor constructs (SAM-Spinach and Vc2-Spinach RNAs) have reduced fluorescence compared to Spinach alone. Fluorescence induction of the WT Vc2-Spinach biosensor is higher than that of the published SAM-Spinach biosensor. Fluorescence of all RNAs decreases with higher temperature. The fluorescence of WT Vc2-Spinach is sensitive to changes in Mg^{2+} concentration between 3 and 10 mM, which is consistent with observations for the Vc2 aptamer,[5] whereas the fluorescence of the Spinach aptamer is unchanged in the same conditions. Furthermore, raising the temperature from 25 °C to 37 °C has a slightly larger effect on the fluorescence of WT Vc2-Spinach than decreasing the Mg^{2+} concentration from 10 mM to 3 mM. Thus, we expect both parameters to influence the binding affinity of the biosensor.

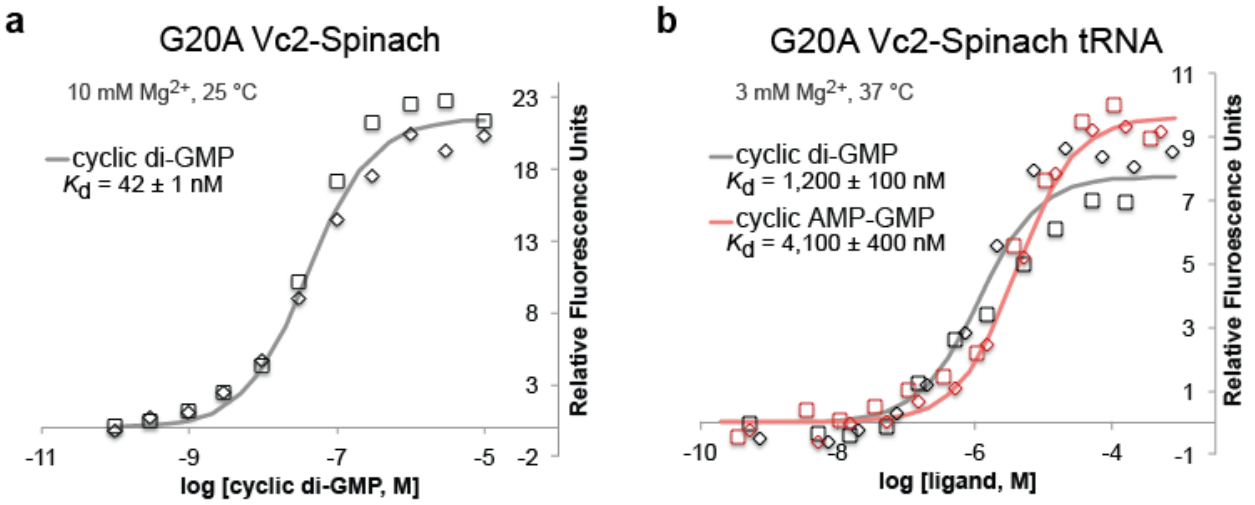

Figure S5. Effect of temperature, Mg^{2+} concentration, and tRNA scaffold on the affinity of G20A Vc2-Spinach. (a) Analysis of G20A Vc2-Spinach binding to cyclic di-GMP at 25 °C in 40 mM HEPES, pH 7.5, 125 mM KCl, and 10 mM $MgCl_2$. RNA (10 nM) was incubated with DFHBI (10 μM) and different concentrations of cyclic di-GMP. (b) Analysis of G20A Vc2-Spinach tRNA binding to cyclic di-GMP and cyclic AMP-GMP at 37 °C in 40 mM HEPES, pH 7.5, 125 mM KCl, and 3 mM $MgCl_2$. RNA (30 nM) was incubated with DFHBI (10 μM) and different concentrations of cyclic di-nucleotide. For (a) and (b), data from two independent replicates of duplicate samples and the best-fit curve are shown. Background fluorescence (without cyclic di-nucleotide) was subtracted from all data points.

As seen in Figure S3, lowering the temperature and increasing the concentration of Mg^{2+} decreases the apparent K_d value of the G20A Vc2-Spinach aptamer for cyclic di-GMP. The apparent K_d of G20A Vc2-Spinach for cyclic di-GMP is 42 ± 1 nM at 25 °C in buffer containing 10 mM $MgCl_2$, compared to 1000 ± 150 nM at 37 °C in buffer containing 3 mM $MgCl_2$. This is likely due to increased folding stability of the RNAs at a lower temperature and with higher Mg^{2+}, as discussed in the main text. The addition of the tRNA scaffold to the G20A Vc2-Spinach sequence appears to have no significant effect on the measured K_d.

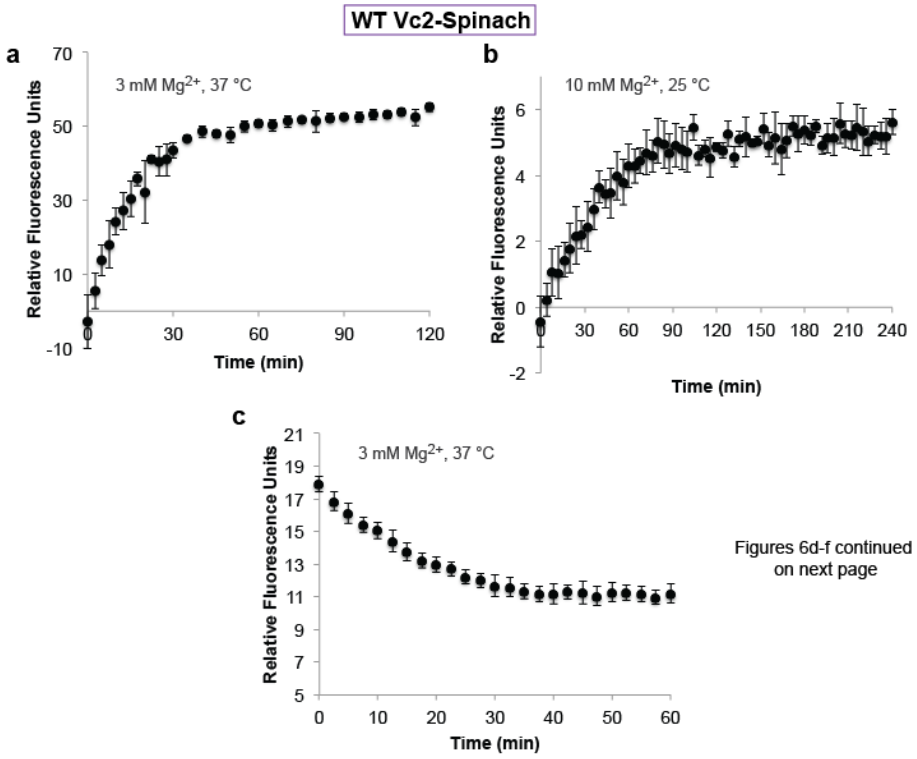

Figure S6. Activation and deactivation of the Vc2-Spinach aptamers. (a) Fluorescence activation rate of WT Vc2-Spinach with cyclic di-GMP at 37 °C. RNA (100 nM) was mixed with DFHBI (10 μM) and cyclic di-GMP (100 μM) in 40 mM HEPES, pH 7.5, 125 mM KCl, and 3 mM $MgCl_2$. (b) Fluorescence activation rate of WT Vc2-Spinach with cyclic di-GMP at 25 °C. RNA (3 nM) was mixed with DFHBI (10 μM) and cyclic di-GMP (100 μM) in 40 mM HEPES, pH 7.5, 125 mM KCl, and 10 mM $MgCl_2$. (c) Fluorescence deactivation of WT Vc2-Spinach at 37 °C. RNA (100 nM) was incubated with DFHBI (10 μM) and cyclic di-GMP (10 μM) in 40 mM HEPES, pH 7.5, 125 mM KCl, and 3 mM $MgCl_2$ (data not shown). The fluorescence was monitored after the RNA was passed through a buffer exchange column equilibrated in buffer without cyclic di-GMP. Control samples where the column was pre-equilibrated with cyclic di-GMP show a decrease of less than 2 RFUs over the course of the experiment. For (a)-(c), error bars represent standard deviation of two replicate samples.

Full activation of WT Vc2-Spinach by ligand binding takes 40 min at 37 °C and 80 min at 25 °C. Conversely, WT Vc2-Spinach is fully deactivated within 40 min at 37 °C. It appears that the current biosensor achieves 75% activation or deactivation in half the time to reach full activation (20 min at 37 °C). The relatively slow response time is due to the slow ligand association and dissociation rates for the Vc2 aptamer.[6] While the YcgR protein-based biosensor displays much faster activation kinetics (1-2 min), the redistribution of cyclic di-GMP during cell division was monitored over the course of 2 h in 15 min intervals.[7] Thus, the Vc2-Spinach biosensor already may be suitable for similar purposes. More generally, though, the timescale of cyclic di-GMP signaling processes has not been studied in depth. We are currently working to improve the binding kinetics of the RNA-based biosensor.

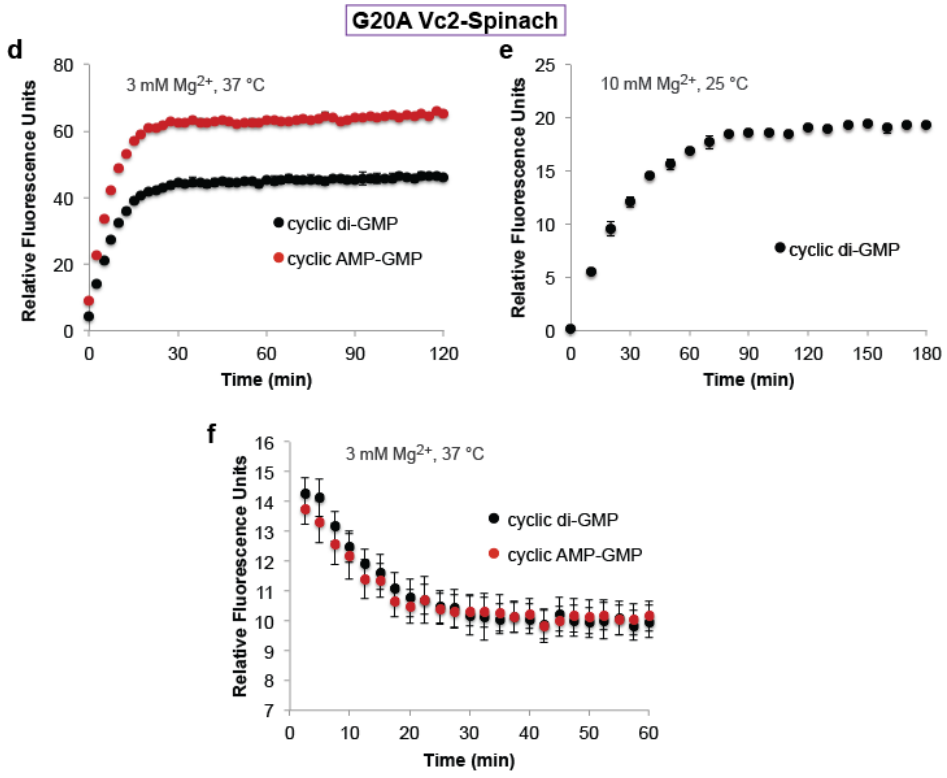

Figure S6 [cont.]. (d) Fluorescence activation rate of G20A Vc2-Spinach with cyclic di-GMP (black) and cyclic AMP-GMP (red) at 37 °C. RNA (100 nM) was mixed with DFHBI (10 μM) and ligand (100 μM) in 40 mM HEPES, pH 7.5, 125 mM KCl, and 3 mM $MgCl_2$. (e) Fluorescence activation rate of G20A Vc2-Spinach with cyclic di-GMP at 25 °C. RNA (10 nM) was mixed with DFHBI (10 μM) and cyclic di-GMP (100 μM) in 40 mM HEPES, pH 7.5, 125 mM KCl, and 10 mM $MgCl_2$. (f) Fluorescence deactivation of G20A Vc2-Spinach at 37 °C. RNA (100 nM) was incubated with DFHBI (10 μM) and either cyclic di-GMP (10 μM, black) or cyclic AMP-GMP (10 μM, red) in 40 mM HEPES, pH 7.5, 125 mM KCl, and 3 mM $MgCl_2$ (data not shown). The fluorescence was monitored after the RNA was passed through a buffer exchange column equilibrated in buffer without cyclic di-nucleotide. Control samples where the column was pre-equilibrated with cyclic di-nucleotide show a decrease of less than 4 RFUs over the course of the experiment. For (d)-(f), error bars represent standard deviation of two replicate samples.

Full activation of G20A Vc2-Spinach by ligand binding takes approx. 25 min at 37 °C and 80 min at 25 °C. Conversely, G20A Vc2-Spinach is fully deactivated within 30 min at 37 °C. It appears that the current biosensor achieves 75% activation or deactivation in half the time to reach full activation (~12.5 min at 37 °C). Little is known about the kinetics of cyclic AMP-GMP signaling and whether these are relevant time scales, but we are currently working to improve the binding kinetics of the RNA-based biosensor.

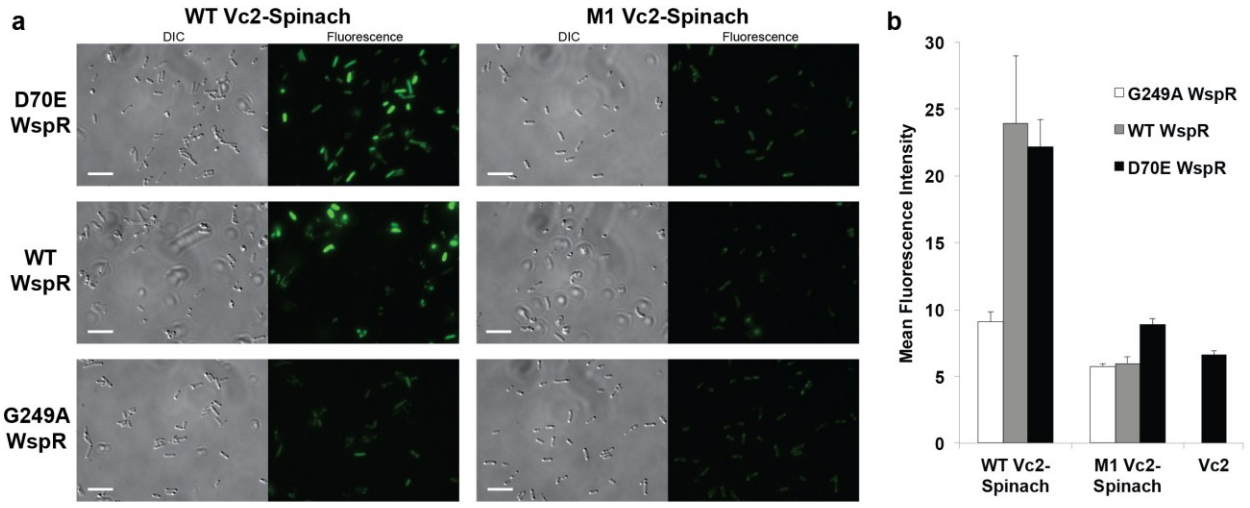

Figure S7. Independent replicate of fluorescence microscopy experiments from Figure 2. (a) Differential interference contrast and fluorescence images of *E. coli* cells expressing WT (left panels) or M1 (right panels) Vc2-Spinach tRNA and WspR variants after incubation with DFHBI. Scale bars represent 10 μm. (b) Mean fluorescence intensity of cells expressing WT or M1 Vc2-Spinach tRNA and various alleles of WspR. Error bars indicate S.E.M. for at least 50 cells.

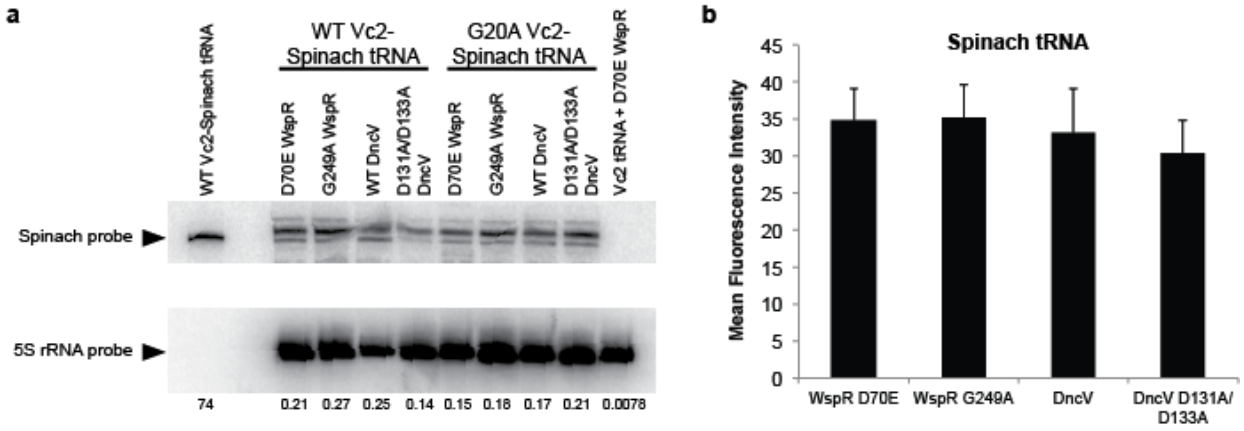

Figure S8. Expression levels of the RNA biosensors and Spinach are unchanged by expression of different enzyme variants. (a) Northern blot analysis of total RNA isolated from cells co-expressing Vc2-Spinach tRNAs and WspR or DncV. *In vitro* transcribed WT Vc2-Spinach tRNA served as a positive control for the Spinach probe; it is expected to be shorter than the *in vivo* RNA product, which contains a terminator sequence. Total RNA isolated from cells co-expressing Vc2 tRNA and D70E WspR served as a negative control for the Spinach probe. 5S rRNA served as the loading control. The ratio of signal intensities for the Spinach probe to the 5S rRNA probe is shown for each lane below the Northern blot. (b) Quantitation of mean fluorescence intensity of cells expressing Spinach tRNA and different alleles of WspR or DncV. Error bars represent the S.E.M. of at least 70 cells.

The effect of co-expression of different enzyme variants on the levels of the RNA constructs was analyzed by Northern blot and fluorescence microscopy. Northern blot analysis shows that the expression of enzymes D70E WspR, G249A WspR, or WT DncV has negligible effect on RNA biosensor levels, whereas D131A/D133A DncV expression has inconsistent effects that are less than 2-fold. Furthermore, we analyzed the fluorescence of cells co-expressing different enzyme variants and the Spinach tRNA, which should exhibit fluorescence independent of cyclic di-nucleotide levels. As expected, these results show that expression of the enzymes has no significant effect on the mean fluorescence intensity of the cells ($p > 0.4$ for all comparisons). Taken together, these data show that the slight differences in RNA levels are not sufficient to account for the fluorescence changes observed for the biosensors under these conditions.

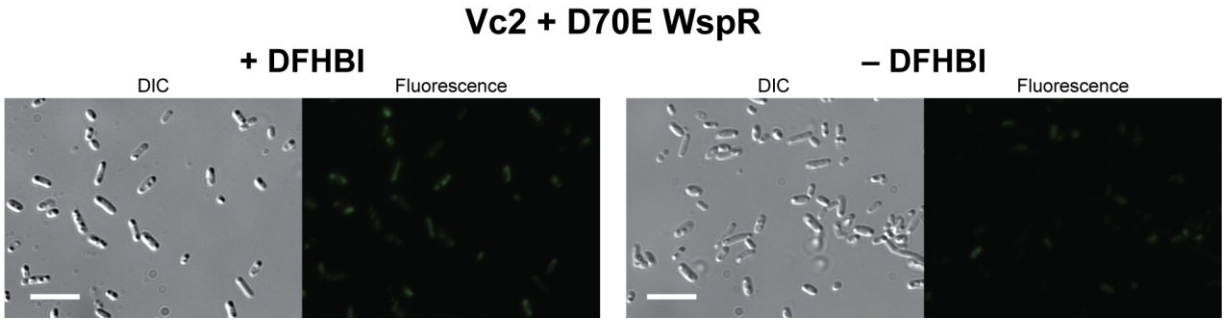

Figure S9. Analysis of non-specific background fluorescence. Differential interference contrast and fluorescent images of *E. coli* cells expressing Vc2 tRNA and the constitutively active D70E WspR after incubation with or without DFHBI. Scale bars represent 10 μm.

Non-specific fluorescence from DFHBI is seen in the negative control that consists of *E. coli* expressing RNA not containing the Spinach aptamer sequence. Comparison of cells expressing Vc2 tRNA and D70E WspR with and without DFHBI showed weak, localized fluorescence only with DFHBI that coincide with the location of inclusion bodies, whereas uniform background fluorescence was observed without DFHBI. This difference was observed only in the fluorescence channel monitoring DFHBI emission.

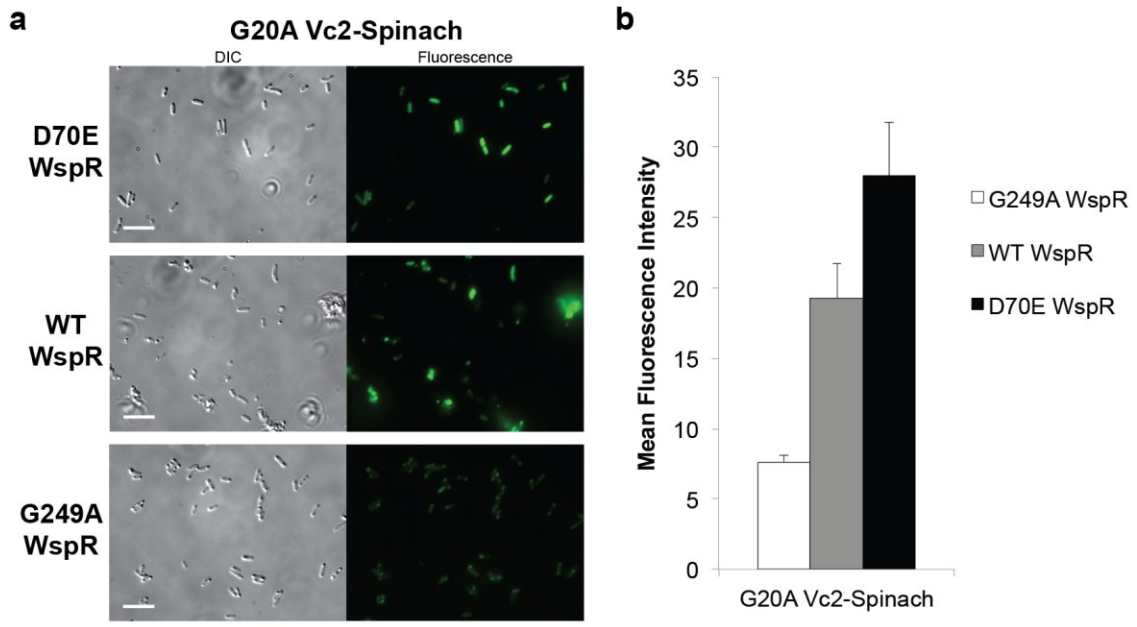

Figure S10. G20A Vc2-Spinach biosensor also responds to cyclic di-GMP. (a) Differential interference contrast (left panels) and fluorescent images (right panels) of *E. coli* cells expressing G20A Vc2-Spinach tRNA and WspR variants after incubation with DFHBI. Scale bars represent 10 μm. (b) Mean fluorescence intensity of cells expressing G20A Vc2-Spinach tRNA and various alleles of WspR. Error bars indicate S.E.M. of at least 50 cells per sample.

The G20A biosensor exhibits an intermediate fluorescence signal in response to expression of WT WspR. This suggests that, in contrast to the WT biosensor, it is not saturated by the levels of cyclic di-GMP produced by WT WspR *in vivo*. The result is consistent with G20A Vc2-Spinach having a poorer affinity for cyclic di-GMP than WT Vc2-Spinach (K_d of 1000 ± 150 nM versus 230 ± 50 nM). We assume that the G20A biosensor is saturated with cyclic di-GMP upon expression of D70E WspR, which produces cyclic di-GMP at concentrations estimated to be around 3 mM.[8] Background fluorescence is observed for cells expressing the G20A biosensor and G249A WspR (inactive variant), consistent with reduced sensitivity leading to no signal in response to endogenous cyclic di-GMP levels.

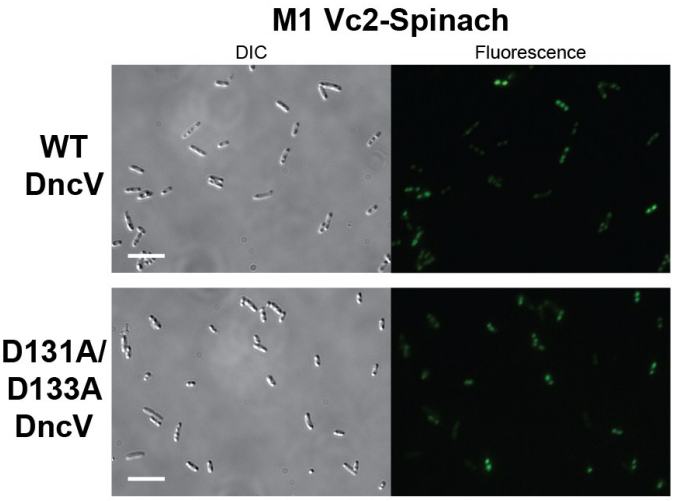

Figure S11. M1 Vc2-Spinach tRNA control shows background fluorescence with WT or D131A/D133A DncV. Differential interference contrast (left panels) and fluorescent images (right panels) of *E. coli* cells expressing M1 Vc2-Spinach tRNA and WT or inactive D131A/D133A DncV after incubation with DFHBI. Quantitation of mean fluorescence intensity of this sample is shown in Figure 3c. Scale bars represent 10 μm.

Weak, localized spots of fluorescence are observed with the M1 Vc2-Spinach biosensor under these conditions, which resemble the non-specific fluorescence of the negative control (Figure S9).

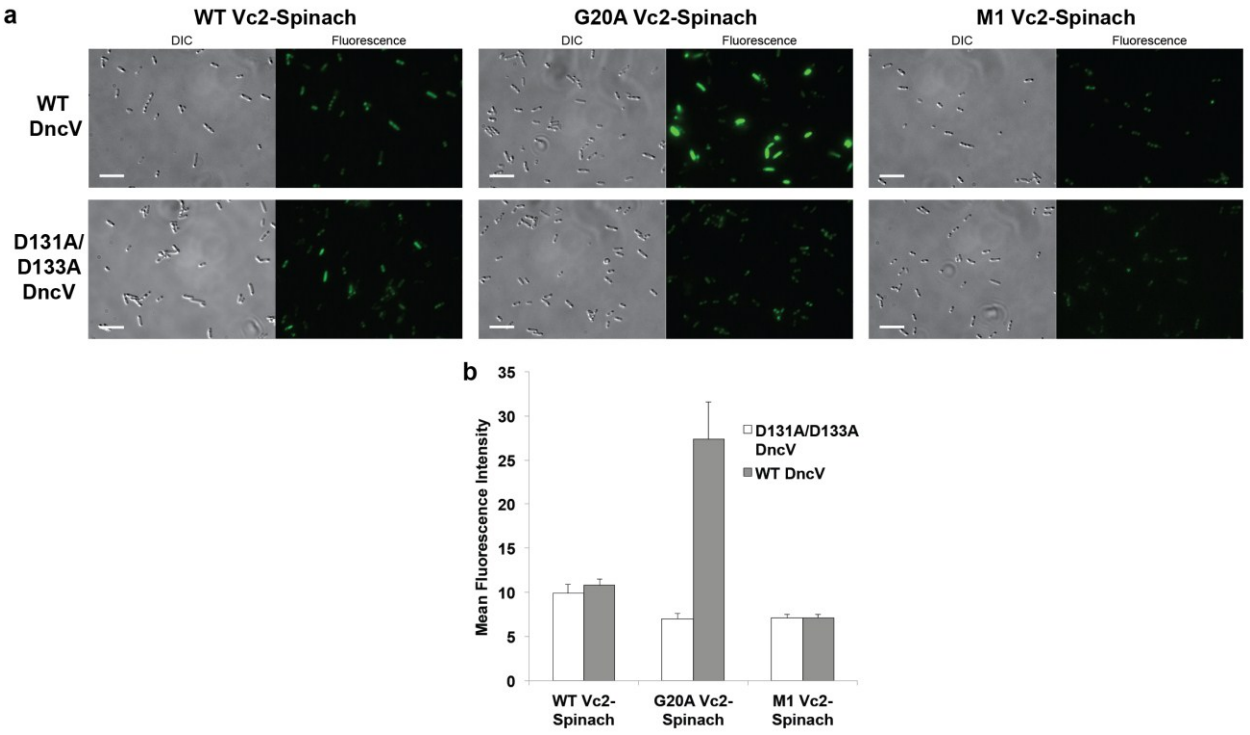

Figure S12. Independent replicate of fluorescence microscopy experiments from Figure 3. (a**)** Differential interference contrast and fluorescence images of *E. coli* cells expressing WT (left panels), G20A (center panels), or M1 (right panels) Vc2-Spinach tRNA and DncV variants after incubation with DFHBI. Scale bars represent 10 μm. (b) Mean fluorescence intensity of cells expressing WT, G20A, or M1 Vc2-Spinach tRNA and various alleles of DncV. Error bars indicate S.E.M. for at least 50 cells.

Figure S13. ^{1}H and ^{13}C NMR spectra for compounds 5 and 6. Resonance assignments were made using COSY, ^{1}H-^{13}C HSQC, ROESY, and ^{1}H-^{13}C HMBC.

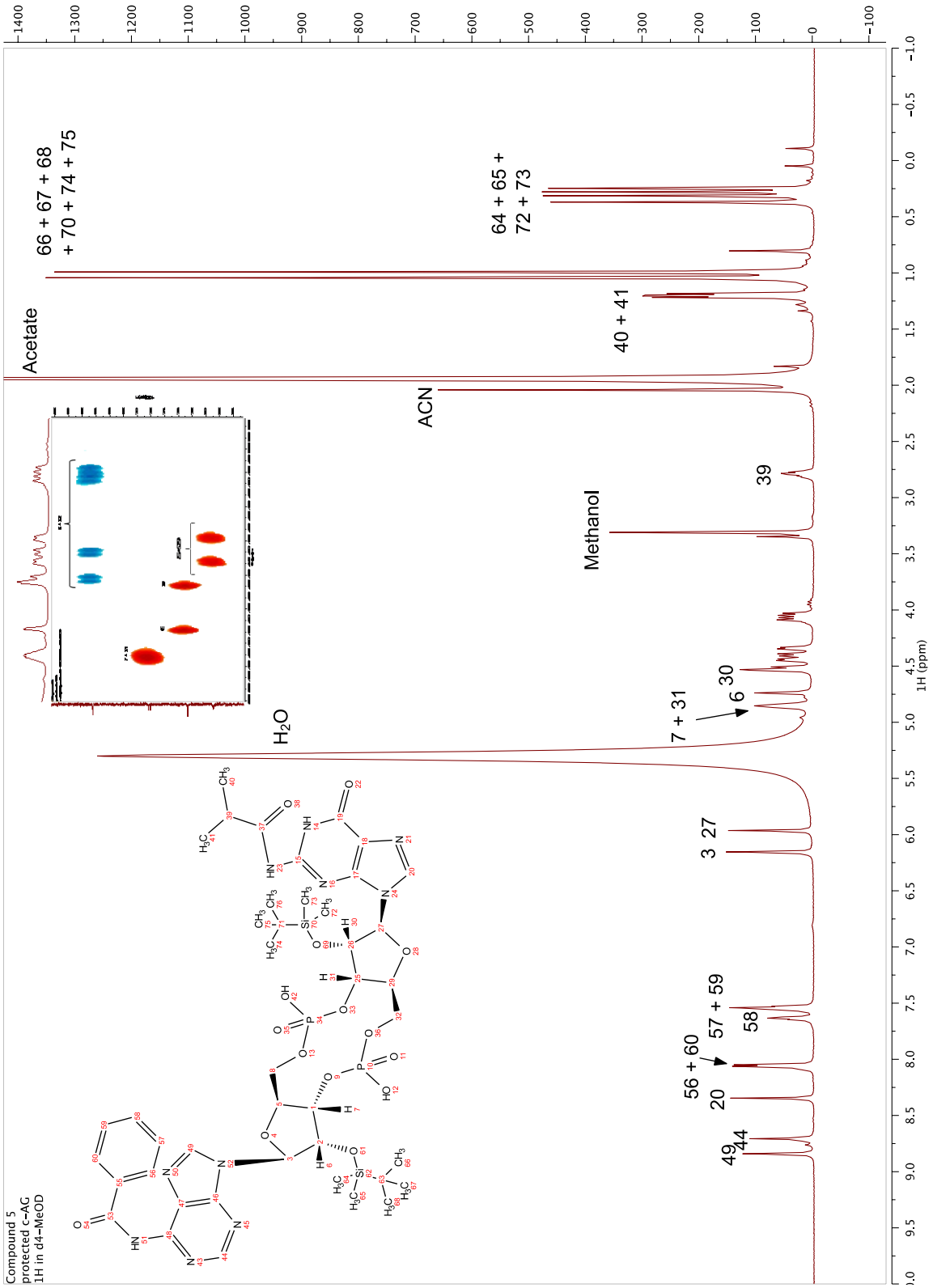

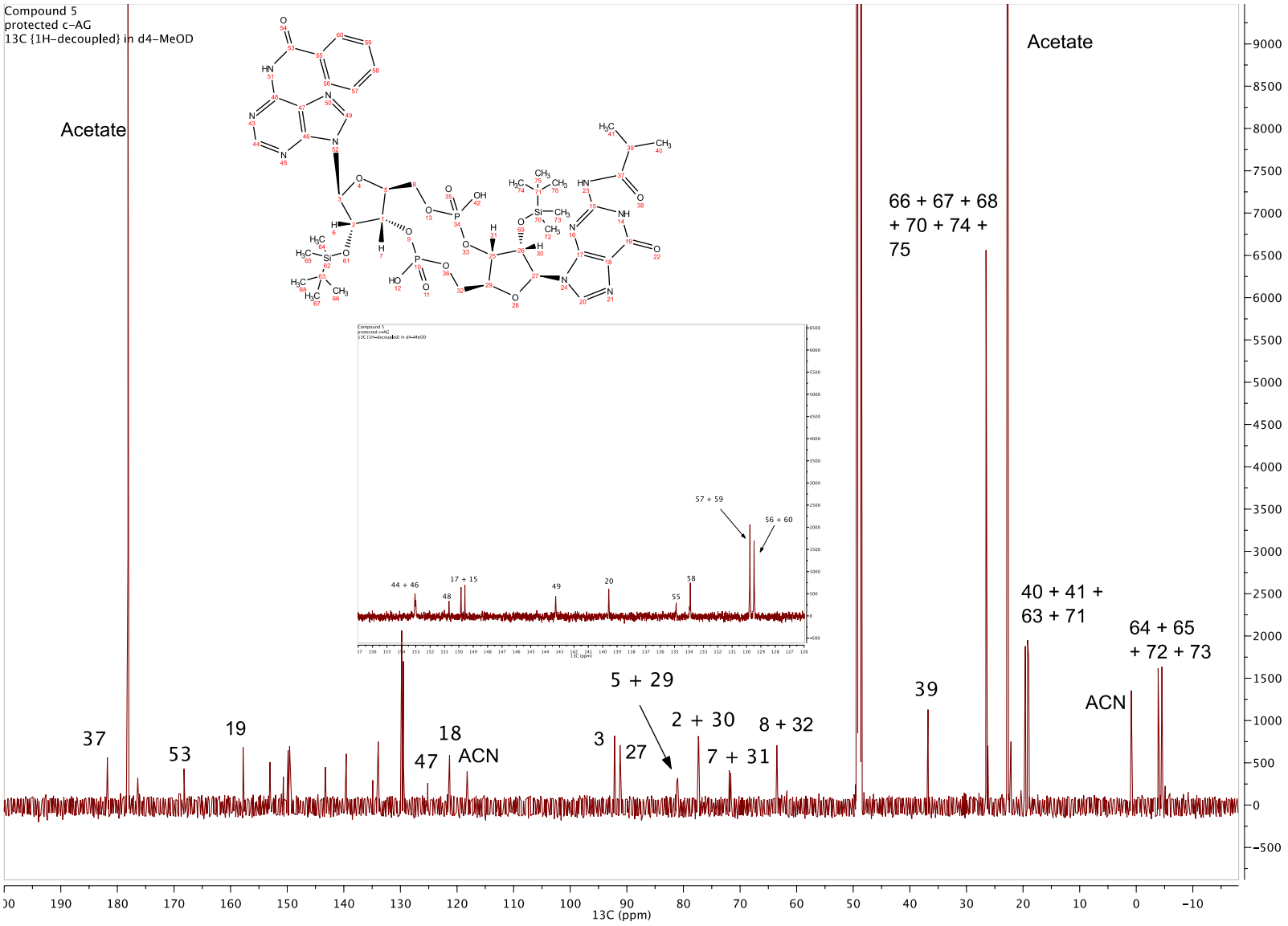
Compound 5
protected c-AG
13C {1H-decoupled} in d4-MeOD
Acetate
Acetate
66 + 67 + 68
+ 70 + 74 +
75
40 + 41 +
63 + 71
64 + 65
+ 72 + 73
39
ACN
5 + 29
2 + 30
8 + 32
7 + 31
3
27
37
53
19
47
18
ACN
57 + 59
56 + 60
44 + 46
48
17 + 15
49
20
55
58
13C (ppm)

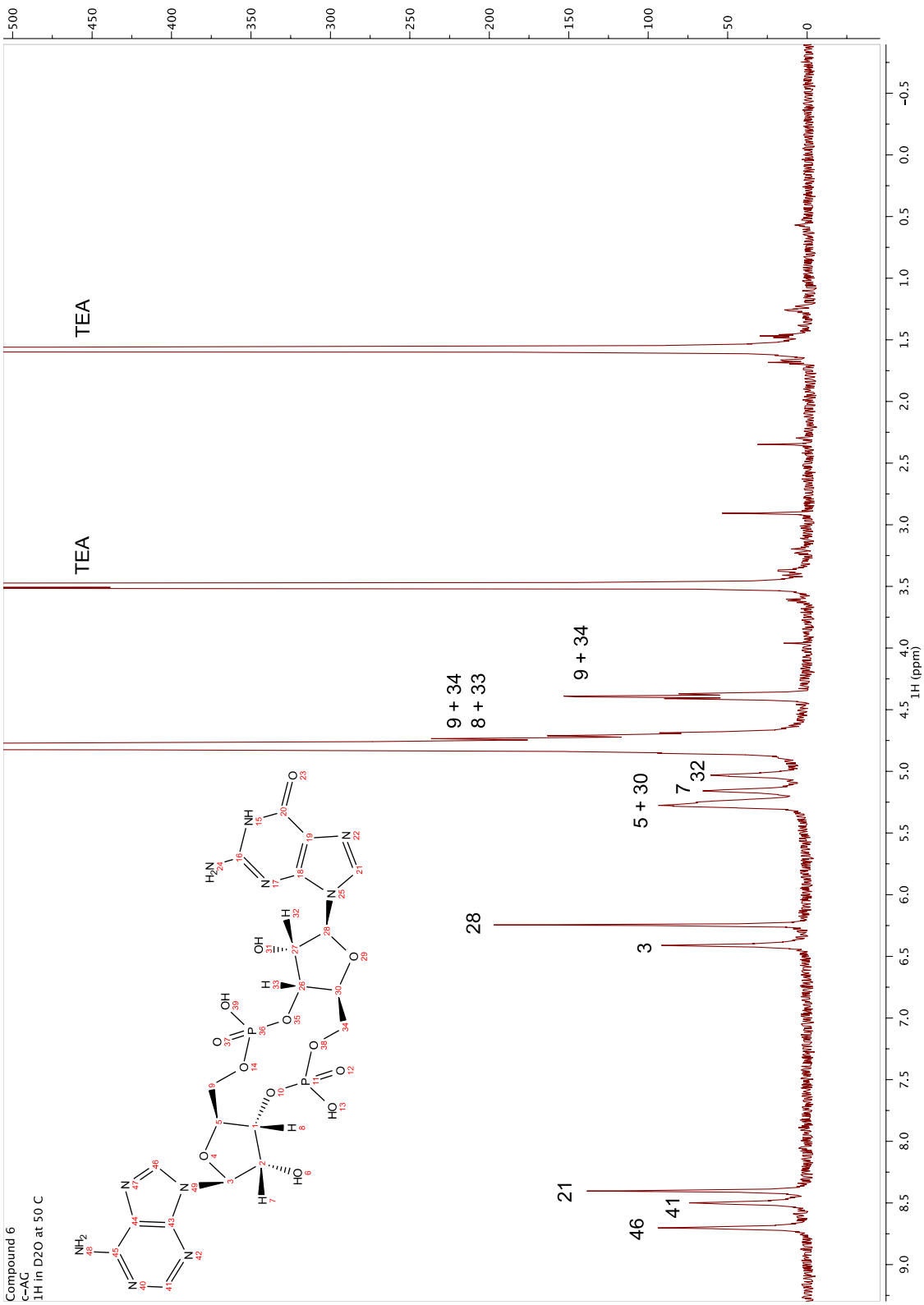
Compound 6
c-AG
1H in D2O at 50 C
TEA
TEA
9 + 34
8 + 33
9 + 34
28
21
46
41
3
5 + 30
7
32
1H (ppm)

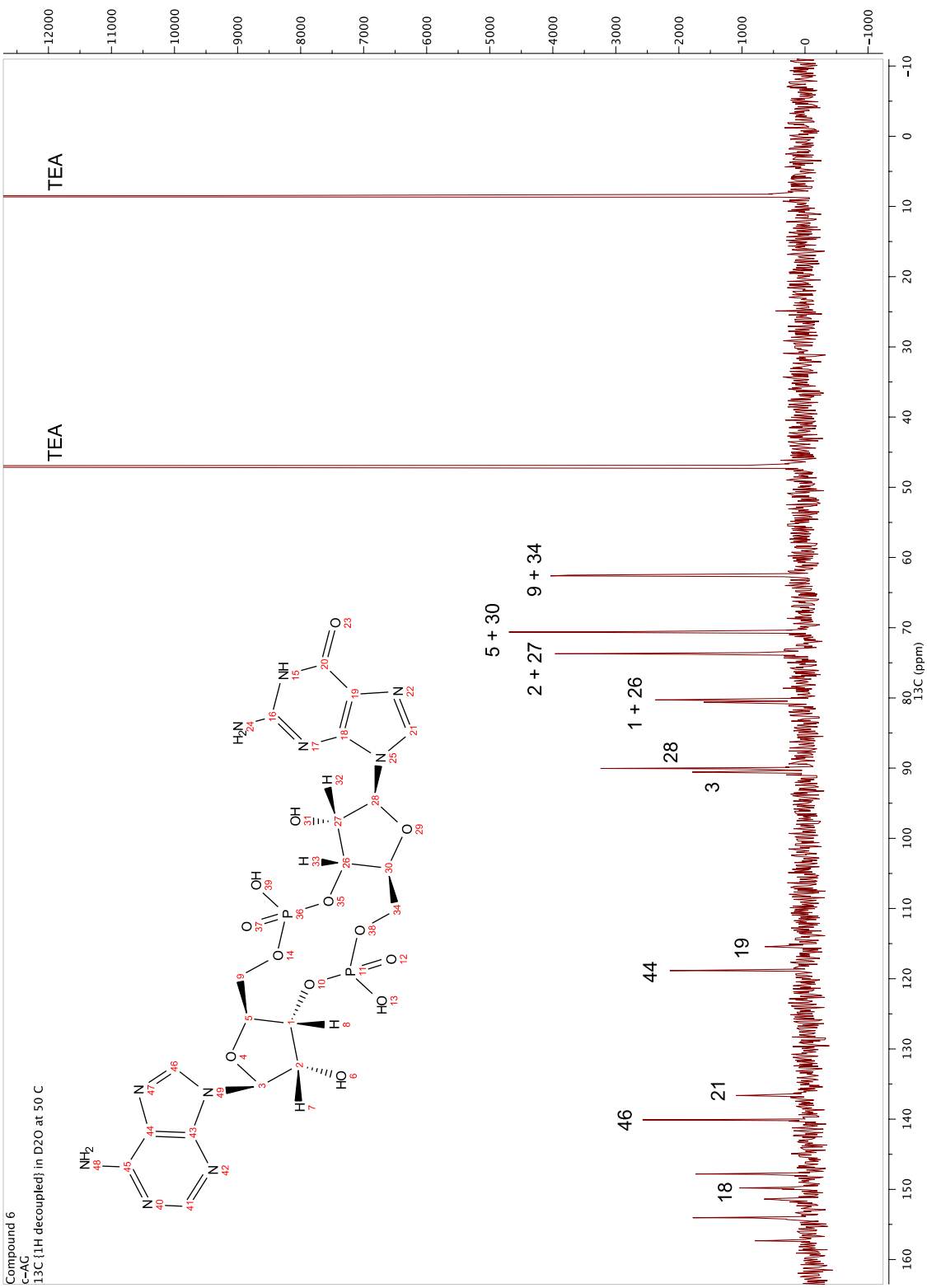
Compound 6
c-AG
13C {1H decoupled} in D2O at 50 C
TEA
TEA
9 + 34
5 + 30
2 + 27
1 + 26
28
3
44
19
46
21
18
13C (ppm)

Table S1. Sequences of DNA primers used in this study. The T7 polymerase promoter sequence is italicized and restriction enzyme sites are underlined.

#	DNA Sequence (5' to 3')	Purpose
1	CCAAG*TAATACGACTCACTATA*GACGCGACTGAATGAAA TGGTGAAGG	*In vitro* transcription of Vc2-Spinach, includes T7 promoter
2	GACGCGACTAGTTACGGAGCTCACAC	*In vitro* transcription of Vc2-Spinach
3	CGGGTCCACACGCACAGAGCAAACCATTCGAAAG	Quikchange to make G20A Vc2-Spinach
4	CACTCTTTCGAATGGTTTGCTCTGTGCGTGTGGAC	Quikchange to make G20A Vc2-Spinach
5	GGTAGGTAGCGGGGTTATCGATGGCAAAATGC	Quikchange to make C92U Vc2-Spinach
6	GCATTTTGCCATCGATAACCCCGCTACCTACC	Quikchange to make C92U Vc2-Spinach
7	ACGCACAGGGCAAACCTGTCGAAAGAGTGGGACG	Quikchange to make M1 Vc2-Spinach
8	CGTCCCACTCTTTCGACAGGTTTGCCCTGTGCGT	Quikchange to make M1 Vc2-Spinach
9	CAGTCAAGATCTCGATCCCGCGAAAT*TAATACGACTCAC TATA*GGG	Constructing pET31b WT-Vc2-Spinach tRNA
10	CATCAGCTCGAGCAAAAAACCCCTCAAGACCCGTTTAGA GGCCCCAAGGGGTTATGCTA	Constructing pET31b WT-Vc2-Spinach tRNA
11	CGATCCCGCGAAAT *TAATACGACTCACTATA*GGG GCCCGGATAGCTCAGTCGGTAGAGCAGCGGCCG GACGCGACTGAATGAAATGGTGAAGGACGGG	Constructing pET31b WT Vc2-Spinach tRNA
12	AGAGGCCCCAAGGGGTTATGCTATGGCGCCCGAACAGG GACTTGAACCCTGGACCCGCGGCCGGACGCGACTAGTT ACGGAGCTCACACTCTACTC	Constructing pET31b WT Vc2-Spinach tRNA
13	GATCCGGCCGGACGCGACTGAATGAAATGGTG	Constructing pET31b Vc2-Spinach tRNA variants
14	CATGCCGCGGCCGGACGCGACTAGTTACGGAGCTC	Constructing pET31b Vc2-Spinach tRNA variants
15	GATCCGGCCGCACGCACAGGGCAAACCATTC	Constructing pET31b Vc2 tRNA
16	CATGCCGCGGCCGCATCGGTAACCCCGCTACC	Constructing pET31b Vc2 tRNA
17	CTTGCATATGCACAACCCTCATGAGAGCAAG	Constructing pET24a D70E WspR
18	CATGCTCGAGTCAGCCCGCCGGGGC	Constructing pET24a D70E WspR
19	ATCCTCCAGGACCTGGTGATGCCCGGCG	Quikchange to make pET24a WT WspR
20	GGCATCACCAGGTCCTGGAGGATCACCG	Quikchange to make pET24a WT WspR
21	TCGGTACGGCGCCGAGGAGTTCGCCATG	Quikchange to make pET24a G249A WspR
22	CGAACTCCTCGGCGCCGTACCGAGCCGC	Quikchange to make pET24a G249A WspR
23	ATCGGCTAGCATGACTTGGAACTTTCACCAGTAC	Constructing pET24a DncV
24	TGCCTCGAGTCAGTGGTGATGATGGTGATGACCACC GCCACTTACCATTGTGCTGCTGAT	Constructing pET24a DncV
25	CCGTTTCAGCCTGGTCAAGAAATGGCTATTGCTGATGGA ACCTATATGCCAATG	Quikchange to make pET24a D131A/D133A DncV
26	CATTGGCATATAGGTTCCATCAGCAATAGCCATTTCTTGA CCAGGCTGAAACGG	Quikchange to make pET24a D131A/D133A DncV

References

(1) Gaffney, B. L.; Veliath, E.; Zhao, J.; Jones, R. A. *Org. Lett.* **2010**, *12*, 3269.

(2) Paige, J. S.; Nguyen-Duc, T.; Song, W.; Jaffrey, S. R. *Science* **2012**, *335*, 1194.

(3) Ponchon, L.; Dardel, F. *Nat. Methods* **2007**, *4*, 571.

(4) Paige, J. S.; Wu, K. Y.; Jaffrey, S. R. *Science* **2011**, *333*, 642.

(5) Kulshina, N.; Baird, N. J.; Ferré-D'Amaré, A. R. *Nat. Struct. Mol. Biol.* **2009**, *16*, 1212.

(6) Smith, K. D.; Lipchock, S. V; Ames, T. D.; Wang, J.; Breaker, R. R.; Strobel, S. A. *Nat. Struct. Mol. Biol.* **2009**, *16*, 1218.

(7) Christen, M.; Kulasekara, H. D.; Christen, B.; Kulasekara, B. R.; Hoffman, L. R.; Miller, S. I. *Science* **2010**, *328*, 1295.

(8) Nakayama, S.; Kelsey, I.; Wang, J.; Roelofs, K.; Stefane, B.; Luo, Y.; Lee, V. T.; Sintim, H. O. *J. Am. Chem. Soc.* **2011**, *133*, 4856.